DALTON
FULL PAPER

Solution NIR CD and MCD in 4f–4f transitions of a series of chiral 3d–4f dinuclear complexes: X-ray structures of (Λ-Δ)-[$(acac)_2Cr^{III}(\mu\text{-}ox)Ln^{III}(HBpz_3)_2$] (Ln = Sm, Ho and Er)†

Md. Abdus Subhan, Takayoshi Suzuki and Sumio Kaizaki*

Department of Chemistry, Graduate School of Science, Osaka University, Toyonaka, Osaka, 560-0043, Japan. E-mail: kaizaki@chem.sci.osaka-u.ac.jp

Received 27th September 2001, Accepted 23rd January 2002
First published as an Advance Article on the web 8th March 2002

A series of stereospecifically assembled configurational chiral heterometal dinuclear 3d–4f complexes (Λ-Δ)-[$(acac)_2$-Cr(ox)Ln$(HBpz_3)_2$] ($acac^-$ = acetylacetonate, ox^{2-} = oxalate, $HBpz_3^-$ = hydrotris(pyrazol-1-yl)borate; Ln(III) = La, Nd, Sm, Ho, Er and Tm: (Λ-Δ)-Cr(ox)Ln, where (Λ-Δ) implies the absolute configuration around the Cr and Ln moieties, respectively) was synthesized and three of them (Sm, Ho and Er) were structurally characterized by X-ray analysis. The (Λ-Δ)-Cr(ox)Ln (Ln = Ho, Er and Yb) complexes crystallize in the identical space group $P2_12_12_1$, whereas the (Λ-Δ)-Cr(ox)Sm complex crystallizes in the monoclinic space group $P2_1$. The absolute configurations of all of the Ln complexes were found to be identical with one another. Near infrared circular dichroism (NIR CD) spectra in the 4f–4f transitions of the (Λ-Δ)-Cr(ox)Ln (Ln = Nd, Sm, Ho, Er and Tm) complexes were studied for the first time in CH_2Cl_2 solution and were compared with those of the previously reported Yb(III) and Dy(III) ions in the (Λ-Δ)-Cr(ox)Ln. The dissymmetry factors g (= $\Delta\varepsilon/\varepsilon$) of the NIR CD for the 4f–4f transitions of these complexes were found to be of the order of 10^{-3} and 10^{-4}, confirming the stereospecific formation and retention of the configurational chirality around the Ln(III) ions of the (Δ-Λ)-Cr(ox)Ln complexes in solution. The solution NIR magnetic circular dichroism (MCD) spectra of the Cr(ox)Ln complexes (Ln = Nd, Sm, Dy, Ho, Er and Tm) were also studied in conjunction with the NIR CD spectra.

Introduction

The near infrared chiroptical method is a sensitive tool for investigating the stereochemical and electronic structural details of Ln(III) ions. For investigating the interactions between chiral biomolecules and lanthanide ions to get an insight into the metalloprotein site (*e.g.*, Ca^{2+} binding site), rigid chiral lanthanide complexes in solution are of prime importance. There have been several studies on circular dichroism (CD) of configurational chiral Ln(III)[1,2] complexes and MCD (magnetic circular dichroism) studies of some Ln(III) complexes in solution and solid state in the visible to near infrared (NIR) region shorter than 800 nm.[2–6] Circular polarization in luminescence (CPL) of the chiral lanthanide complexes[7–9] has also been studied recently. Accurate analysis of solution chiroptical spectra is difficult to make due to the labile and poorly defined structures in Ln(III) systems. Very recently, two examples with rigid structures have been reported. On one hand, the solution structure and dynamics[10] of two chiral Yb(III) mononuclear complexes with C_4 symmetric chiral DOTMA (1*R*,4*R*,7*R*,10*R*-α,α′,α″,α‴-tetramethyl-1,4,7,10-tetraazacyclododecane-1,4,7,10-tetraacetic acid) ligands based on cyclen are completely defined by NIR CD, NMR and luminescence study.[11] On the other hand, our more recent paper[12] of NIR CD spectra for the 4f–4f transitions concerns the configurational chiral 3d–4f (Λ-Δ)-Cr(ox)Ln (Ln = Dy and Yb) complexes containing two tris(pyrazol-1-yl)borates with no asymmetric carbons (Scheme 1), which is the second report on the NIR CD of the Yb(III) complex, but the first one on that of the Dy(III) complex. Structurally well characterized 3d–4f heterometal dinuclear complexes are also interesting from the viewpoint of the magnetic interaction and energy transfer between 3d and 4f states.[13] The variation of ionic radii over a series of Ln(III) complexes could vary their stereochemistry as well as the spectroscopic properties, especially in solution. Hence, solution NIR CD of a series of Ln(III) complexes is invaluable for comparison of the structure and properties of the complexes.

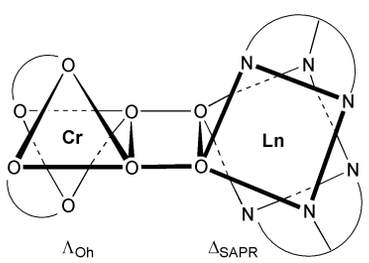

Scheme 1 Schematic view of the complex (Λ-Δ)-[$Cr(acac)_2(ox)$-$Ln(HBpz_3)_2$].

In our present paper we report the synthesis, characterization of configurational chiral 3d–4f (Λ-Δ)-[$(acac)_2Cr(ox)Ln$-$(HBpz_3)_2$] (Ln = La, Nd, Sm, Ho, Er and Tm) complexes along with the X-ray structural analysis of the (Λ-Δ)-Cr(ox)Ln (Sm, Ho and Er) complexes. On the basis of the solution NIR CD and MCD spectra in the 4f–4f transitions, the retention of the configurational chirality around the Ln(III) ions in solution is demonstrated by the dissymmetry factors for the CD in support of the selection rules for 4f–4f optical activity.[14] As an essential feature of the chirality in coordination chemistry, we attempt here to correlate the molecular structure or absolute configuration with solution NIR CD.

† Electronic supplementary information (ESI) available: Fig. S1–3: ORTEP views of the complexes (Λ-Δ)-[$Cr(acac)_2(ox)Ln(HBpz_3)_2$]·$2CH_2Cl_2$ where Ln = Ho and Er respectively; NIR absorption and NIR CD of (Λ-Δ)-[$Cr(acac)_2(ox)Er(HBpz_3)_2$] and NIR MCD of [$Cr(acac)_2$-$(ox)Er(HBpz_3)_2$] in CH_2Cl_2. See http://www.rsc.org/suppdata/dt/b1/b108770c/

 DOI: 10.1039/b108770c

Experimental

Materials

All reagent grade chemicals were used without further purification. The ligand potassium hydrotris(pyrazol-1-yl)borate KHBpz$_3$ was prepared by a similar method to that described by Trofimenko.[15] The optically resolved Λ-(+)$_{540}^{\Delta\varepsilon}$-Na[Cr(acac)$_2$(ox)] complex was obtained as described previously.[12]

Preparation of (Λ-Δ)-[(acac)$_2$Cr(ox)Ln(HBpz$_3$)$_2$]·*n*CH$_2$Cl$_2$ (Ln = La, Nd, Sm, Ho, Er and Tm)

All the (Λ-Δ)-Cr(ox)Ln complexes were prepared by the aqueous method[16] except for the Nd and La complexes. For the complexes Cr(ox)La and Cr(ox)Nd, a slight excess of the complex ligand Λ-Na[Cr(acac)$_2$(ox)] was used. Each aqueous solution of Λ-Na[Cr(acac)$_2$(ox)] and KHBpz$_3$ was separately added to an aqueous solution of LnCl$_3$·6H$_2$O in a beaker. Slow and controlled addition of an aqueous solution of KHBpz$_3$ to LnCl$_3$·6H$_2$O was performed in order to avoid the possible formation of a large amount of Ln(HBpz$_3$)$_3$. The reaction mixture was cooled in a refrigerator for a few hours. The purification and recrystallization of the complexes were carried out according to a previous method.[16] The corresponding racemic Cr(ox)Ln complexes were also prepared by the same method.

Measurements

Absorption spectra were measured on a Perkin Elmer Lambda-19 spectrophotometer. CD data were collected on a Jasco J-720W spectropolarimeter. The AB and CD measurements were made on solutions of concentrations of 0.017 M, 0.016 M, 0.047 M, 0.033 M and 0.051 M of the Cr(ox)Nd, Cr(ox)Sm, Cr(ox)Ho, Cr(ox)Er and Cr(ox)Tm complexes, respectively. MCD spectra of the corresponding racemic complexes were recorded on 0.01 M solutions on a Jasco J-720W spectropolarimeter in a magnetic field of 1.5 T (1 T = 10000 Gauss) with an electromagnet at room temperature. Two ml solutions in methylene chloride were used for each measurement.

Crystal structure determination

A purple polyhedral crystal of each Cr(ox)Ln (Ln = Sm, Ho and Er) complex [(acac)$_2$Cr(ox)Ln(HBpz$_3$)$_2$]·*n*CH$_2$Cl$_2$ was sealed in a glass capillary tube to prevent possible efflorescence. The X-ray intensities ($2\theta_{max}$ = 60°) were measured on a Rigaku AFC-5R or AFC-7R four circle diffractometer and absorption corrections were made by the numerical integration method.[17] The structures were solved by the direct method using the SHELXS86 program,[18] and refined on F^2 against all reflections by the full-matrix least-squares technique using the SHELXL97 program.[19] All non-hydrogen atoms except for those of the solvated dichloromethane molecules were treated anisotropically. All calculations were carried out using the TeXsan software package.[20]

All of the Cr(ox)Ln complexes crystallize in the noncentrosymmetric space groups $P2_1$ (Ln = Sm) or $P2_12_12_1$ (Ln = Ho and Er). The absolute configuration of the complexes was assumed to be (Λ-Δ)-Cr(ox)Ln on the basis of the starting Cr complex used and of the satisfactory Flack[21] parameters.

CCDC reference numbers 171631–171633.

See http://www.rsc.org/suppdata/dt/b1/b108770c/ for crystallographic data in CIF or other electronic format.

Results and discussion

Synthesis of (Λ-Δ)-[(acac)$_2$Cr(ox)Ln(HBpz$_3$)$_2$] (Ln = La and Nd)

As mentioned in our previous paper,[16] the synthetic method was not applicable to the Cr(ox)La and Cr(ox)Nd complexes due to the formation of a large amount of Ln(HBpz$_3$)$_3$, which is highly insoluble in an aqueous medium. The synthesis method for the La and Nd complexes was modified by the slow and controlled addition of KHBpz$_3$ to an aqueous solution of LnCl$_3$·6H$_2$O (see Experimental section). This could open the way for the synthesis of the whole series of Cr(ox)Ln complexes.

The solution stability of the complexes was confirmed by observing the FAB-MS spectra in 1:1 CH$_2$Cl$_2$:MeOH solutions ranging in dilute concentration from 10^{-4} to 10^{-5}M as well as by the observation of no change in the CH$_2$Cl$_2$ solutions even after standing for a few months as previously described for the Cr–Yb and Cr–Dy complexes.[12]

X-Ray structural analysis of (Λ-Δ)-[(acac)$_2$Cr(ox)Ln(HBpz$_3$)$_2$] (Ln = Sm, Ho and Er)

In order to substantiate the dinuclear formation of the (Λ-Δ)-Cr(ox)Ln complexes as predicted by elemental analysis and FAB-MS (Table 1), single crystal X-ray structural analysis for some of the complexes was performed. The crystallographic data for all the complexes are given in Table 2. The ORTEP[22] view of (Λ-Δ)-[(acac)$_2$Cr(ox)Sm(HBpz$_3$)$_2$]·CH$_2$Cl$_2$ is illustrated in Fig. 1 and those of (Λ-Δ)-[(acac)$_2$Cr(ox)Ho(HBpz$_3$)$_2$]·2CH$_2$Cl$_2$ and (Λ-Δ)-[(acac)$_2$Cr(ox)Er(HBpz$_3$)$_2$]·2CH$_2$Cl$_2$ in Fig. 1S and 2S,† respectively.

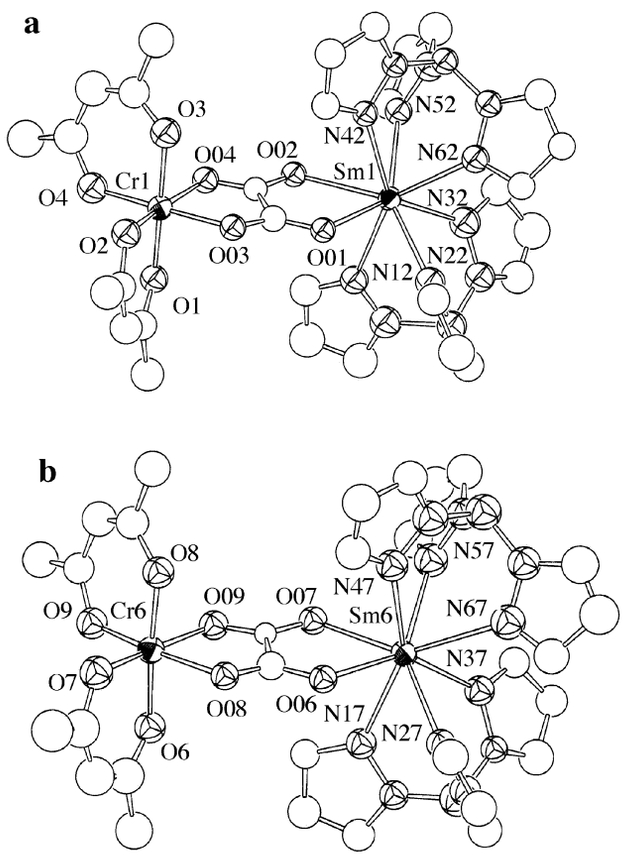

Fig. 1 ORTEP view of the two crystallographically independent molecules of complex (Λ-Δ)-[Cr(acac)$_2$(ox)Sm(HBpz$_3$)$_2$]·CH$_2$Cl$_2$.

Assignment of the chiral space groups as either $P2_1$ (Sm) or $P2_12_12_1$ (Ho and Er) was unequivocal, and the determination of the absolute configuration was conclusive with no indication of racemic twinning. The complexes Cr(ox)Ln (Ln = Ho, Er and Yb) crystallize in the same orthorhombic space group, $P2_12_12_1$. In contrast, the complex (Λ-Δ)-[(acac)$_2$Cr(ox)Sm(HBpz$_3$)$_2$]·CH$_2$Cl$_2$ crystallizes in the monoclinic space group $P2_1$ with Z = 4 with two crystallographically independent complex molecules and two solvated CH$_2$Cl$_2$ molecules in the

Table 1 Elemental analysis and FAB-MS of (Λ-Δ)-[$(acac)_2Cr(ox)Ln(HBpz_3)_2$] complexes

Complex	Yield (%)	Elemental analysis[a] C (%)	H (%)	N (%)	FAB-MS (major fragments) *m*/*z*
$[(acac)_2Cr(ox)La(HBpz_3)_2]\cdot 6CH_2Cl_2\cdot 2C_6H_{14}$	8	38.24 (38.77)	4.78 (4.57)	10.20 (10.29)	904 ($[M + H]^+$, 6%), 564 ($[La(HBpz_3)_2]^+$, 100%)
$[(acac)_2Cr(ox)Nd(HBpz_3)_2]\cdot 4CH_2Cl_2\cdot 2C_6H_{14}$	10	38.81 (38.89)	4.52 (4.97)	11.84 (11.83)	910 ($[M + H]^+$, 3.8%), 570 ($[Nd(HBpz_3)_2]^+$, 100%)
$[(acac)_2Cr(ox)Sm(HBpz_3)_2]\cdot 1.75CH_2Cl_2$	12	35.86 (35.86)	3.46 (3.55)	15.87 (15.18)	916 ($[M + H]^+$, 5%), 576 ($[Sm(HBpz_3)_2]^+$, 100%)
$[(acac)_2Cr(ox)Ho(HBpz_3)_2]\cdot 2CH_2Cl_2$	19	35.13 (34.97)	3.40 (3.48)	15.44 (15.29)	930 ($[M + H]^+$, 11.8%), 591 ($[Ho(HBpz_3)_2]^+$, 100%)
$[(acac)_2Cr(ox)Er(HBpz_3)_2]\cdot 2CH_2Cl_2$	27	34.97 (34.9)	3.48 (3.48)	15.29 (15.26)	933 ($[M + H]^+$, 4%), 593 ($[Er(HBpz_3)_2]^+$, 100%)
$[(acac)_2Cr(ox)Tm(HBpz_3)_2]$	29	38.53 (38.58)	3.68 (3.67)	17.80 (18.01)	934 ($[M + H]^+$, 9.2%), 594 ($[Tm(HBpz_3)_2]^+$, 100%)

[a] Calculated values are given in parentheses.

Table 2 Crystallographic data for (Λ-Δ)-Cr(ox)Sm, (Λ-Δ)-Cr(ox)Ho and (Λ-Δ)-Cr(ox)Er

	(Λ-Δ)-Cr(ox)Sm	(Λ-Δ)-Cr(ox)Ho	(Λ-Δ)-Cr(ox)Er
Formula	$C_{31}H_{36}B_2Cl_2CrN_{12}O_8Sm$	$C_{32}H_{38}B_2Cl_4CrN_{12}O_8Ho$	$C_{32}H_{38}B_2Cl_4CrN_{12}O_8Er$
M	999.59	1099.09	1101.42
T/°C	23	23	23
λ(MoKα)/Å	0.71069	0.71069	0.71069
Crystal system	Monoclinic	Orthorhombic	Orthorhombic
Space group	$P2_1$ (no. 4)	$P2_12_12_1$ (no. 19)	$P2_12_12_1$ (no. 19)
a/Å	23.252(7)	15.571(3)	15.552(3)
b/Å	15.228(5)	21.326(4)	21.287(4)
c/Å	12.142(3)	14.190(3)	14.191(3)
β/°	89.97(2)	90	90
V/Å^3	4299(2)	4712.0(17)	4698.1(15)
Z	4	4	4
ρ_{calc}/g cm^{-3}	1.557	1.544	1.549
μ(MoKα)/cm^{-1}	17.89	21.81	22.9
$R1(F^2)$	0.0524	0.0235	0.046
$wR2(F^2)$	0.1624	0.1429	0.1446

Table 3 Selected bond lengths (Å) and bond angles (°) for (Λ-Δ)-Cr(ox)Sm, (Λ-Δ)-Cr(ox)Ho and (Λ-Δ)-Cr(ox)Er

(Λ-Δ)-Cr(ox)Sm				(Λ-Δ)-Cr(ox)Ho		(Λ-Δ)-Cr(ox)Er	
Sm(1)–O(01)	2.369(9)	Sm(6)–O(06)	2.489(9)	Ho–O(01)	2.365(8)	Er–O(01)	2.363(6)
Sm(1)–O(02)	2.398(9)	Sm(6)–O(07)	2.381(9)	Ho–O(02)	2.331(8)	Er–O(02)	2.333(6)
Sm(1)–N(12)	2.592(10)	Sm(6)–N(17)	2.664(9)	Ho–N(12)	2.495(11)	Er–N(12)	2.489(8)
Sm(1)–N(42)	2.553(12)	Sm(6)–N(47)	2.603(11)	Ho–N(42)	2.514(10)	Er–N(42)	2.506(8)
Sm(1)–N(22)	2.488(10)	Sm(6)–N(27)	2.509(12)	Ho–N(22)	2.414(11)	Er–N(22)	2.409(7)
Sm(1)–N(52)	2.553(12)	Sm(6)–N(57)	2.474(11)	Ho–N(52)	2.421(11)	Er–N(52)	2.420(8)
Sm(1)–N(32)	2.541(11)	Sm(6)–N(37)	2.508(10)	Ho–N(32)	2.507(10)	Er–N(32)	2.479(7)
Sm(1)–N(62)	2.586(12)	Sm(6)–N(67)	2.479(13)	Ho–N(62)	2.516(11)	Er–N(62)	2.512(8)
C(01)–O(01)	1.235(15)	C(06)–O(06)	1.276(14)	C(01)–O(01)	1.235(15)	C(01)–O(01)	1.220(10)
C(02)–O(02)	1.233(14)	C(07)–O(07)	1.254(15)	C(02)–O(02)	1.248(14)	C(02)–O(02)	1.266(10)
C(01)–O(03)	1.256(16)	C(06)–O(08)	1.261(14)	C(01)–O(03)	1.224(15)	C(01)–O(03)	1.255(10)
C(02)–O(04)	1.232(14)	C(07)–O(09)	1.282(15)	C(02)–O(04)	1.281(15)	C(02)–O(04)	1.277(10)
O(01)–Sm(1)–O(02)	68.7(3)	O(06)–Sm(6)–O(07)	68.0(3)	O(01)–Ho–O(02)	69.0(3)	O(01)–Er–O(02)	69.6(2)
N(12)–Sm(1)–N(22)	73.2(4)	N(17)–Sm(6)–N(27)	71.1(3)	N(12)–Ho–N(22)	76.0(4)	N(12)–Er–N(22)	76.5(3)
N(42)–Sm(1)–N(52)	73.7(4)	N(47)–Sm(6)–N(57)	74.5(4)	N(42)–Ho–N(52)	76.9(4)	N(42)–Er–N(52)	77.2(3)
N(12)–Sm(1)–N(32)	70.7(4)	N(17)–Sm(6)–N(37)	70.0(3)	N(12)–Ho–N(32)	71.2(4)	N(12)–Er–N(32)	70.1(2)
N(42)–Sm(1)–N(62)	71.1(4)	N(47)–Sm(6)–N(67)	72.3(4)	N(42)–Ho–N(62)	71.6(4)	N(42)–Er–N(62)	71.1(3)
N(22)–Sm(1)–N(32)	79.7(4)	N(27)–Sm(6)–N(37)	79.3(4)	N(22)–Ho–N(32)	80.6(4)	N(22)–Er–N(32)	80.4(2)
N(52)–Sm(1)–N(62)	75.1(4)	N(57)–Sm(6)–N(67)	77.3(5)	N(52)–Ho–N(62)	78.3(4)	N(52)–Er–N(62)	78.3(3)

asymmetric unit. The overall molecular structure of these complexes is similar to that for the corresponding Cr(ox)Yb complex: Oh-6-Λ-Cr(III) and SAPR-8-Δ-Ln(III) configurations (Scheme 1).[12]

Table 3 shows the selected bond lengths and bond angles of only the Ln moieties. The bond lengths (Ln–O or Ln–N) increase and the bond angles (O–Ln–O or N–Ln–N) decrease reasonably with the increase of ionic radii (from Yb,[12] Er and Ho to Sm) although there are a few exceptions to be noted probably owing to the crystal packing. The Sm–O bond lengths are longer compared to those of both Ho–O and Er–O, and the same is true for the Ln–N bond lengths. The Ln–N(62) distances are longer than the other Ln–N distances, the only exception being the corresponding Sm(6)–N(67) distance (2.479(13) Å) which is comparable to the Sm(6)–N(57) distance (2.474(11) Å) and shorter compared to the other Sm–N distances as shown in Table 3. The C–O distances of the oxalate ligand for all the complexes lie between the normal ranges for C–O and C=O bonds. The smallest O–Ln–O angle is 68.03° for O(06)–Sm(1)–O(07) and the largest one is 69.62° for O(01)–Er–

Table 4 Values of δ and φ (°) for (Λ-Δ)-Cr(ox)Sm, (Λ-Δ)-Cr(ox)Ho, (Λ-Δ)-Cr(ox)Er and (Λ-Δ)-Cr(ox)Yb

Notation[a]	(Λ-Δ)-Cr(ox)Sm[b]	(Λ-Δ)-Cr(ox)Ho	(Λ-Δ)-Cr(ox)Er	(Λ-Δ)-Cr(ox)Yb
δ_1: O(01)–[N(42)/N(22)]–N(62)	13.68 (14.02)	14.50	14.91	16.44
δ_2: O(02)–[N(12)/N(52)]–N(32)	1.52 (0.98)	6.73	6.829	6.66
δ_3: O(01)–[N(12)/N(22)]–N(32)	59.88 (58.40)	55.18	54.81	54.72
δ_4: O(02)–[N(42)/N(52)]–N(62)	58.06 (60.71)	55.66	55.29	56.06
φ_1: N(22)–O(01)–O(02)–N(52)	37.12 (38.42)	32.32	32.22	24.19
φ_2: N(42)–N(62)–N(32)–N(12)	31.58 (30.35)	27.89	27.45	19.44

[a] The notation is based on ref. 25. δ and φ values for idealized polyhedra: SAPR; $\delta_1 = 0.0$, $\delta_2 = 0.0$, $\delta_3 = 52.5$, $\delta_4 = 52.5$, $\varphi_1 = 24.5$, $\varphi_2 = 24.5°$, DD; $\delta_1 = 29.5$, $\delta_2 = 29.5$, $\delta_3 = 29.5$, $\delta_4 = 29.5$, $\varphi_1 = 0.0$, $\varphi_2 = 0.0°$, TPRS; $\delta_1 = 21.8$, $\delta_2 = 0.0$, $\delta_3 = 48.2$, $\delta_4 = 48.2$, $\varphi_1 = 14.1$, $\varphi_2 = 14.1°$. [b] Values in parentheses indicate the corresponding values for the other crystallographically independent molecule in the unit cell.

O(02), however, the smallest N–Ln–N angle is 70.03° for N(17)–Sm(6)–N(37), and the largest one is 80.64° for N(22)–Ho–N(32). The structural parameters around the Cr(III) moieties show no regular change with the ionic size of the Ln(III) ions.

The values of δ and ϕ, obtained by polytopal analysis, are collected in Table 4. The δ_1 and δ_2 values showing the planarity of the squares for the chiral complexes (Sm, Ho, Er and Yb) are 13.85° and 1.25° (on average), 14.50° and 6.73°, 14.91° and 6.83°, 16.44° and 6.66°, respectively. The δ_1 values increase with decreasing ionic radii. The larger the Ln(III) ion radii, the closer are the values to square antiprismatic (SAPR) geometry. The δ_2 values for the Sm complex are very small compared to the other δ_2 values, which show the irregular changes. The reasonable geometry around the eight coordinate Ln(N_6O_2) seems to be SAPR from the δ and φ values, being on a geometric pathway to DD (dodecahedron) and TPRS (bicapped trigonal prism) as also found for both the chiral and racemic Yb complexes.[12,16]

CD of the d–d transitions of the Cr(III) moiety in the (Λ-Δ)-Cr(ox)Ln complexes

For all the Cr(ox)Ln complexes a major positive CD band with $\Delta\varepsilon = ca.\ +2.9\ M^{-1}\ cm^{-1}$ was observed in the $^4A_2 \longrightarrow {}^4T_2$ d–d transition region around 540 nm, the position of which is shifted to lower frequency due to the coordination of the Ln moiety as observed for the corresponding Yb and Dy complexes.[12] The positive sign of the major CD component shows the retention of the Λ absolute configuration for $[(acac)_2Cr(ox)]^-$ in the Cr(ox)Ln assembly as observed previously for the Cr(ox)Yb and Cr(ox)Dy complexes,[12] and also as confirmed by the X-ray analysis (*vide supra*).

CD in the 4f–4f transitions of Ln(III) in the (Λ-Δ)-Cr(ox)Ln complexes

Multiple CD components are found in the 4f–4f transitions of the Ln(III) ions in the Cr(ox)Ln complexes at room temperature as shown in Figs. 2 and 4–8. There are two important factors for the CD assignments of the Ln complexes: multiplicity of the CD components and variation of the *g* values. The multiplicity of the CD components arises from the crystal field splitting within the $^{2S+1}L_J$ levels split by the interelectronic repulsion and spin–orbit coupling, of which the energy orders have been determined by Carnall *et al.*[23] On the other hand, variation of the dissymmetry factors $g(= \Delta\varepsilon/\varepsilon)$ values is subject to the selection rule for the optical activity of Ln complexes proposed by Richardson.[14] This indicates that the 4f–4f transitions with $\Delta S = 0$; $\Delta L = 0, 1, 3, 6$; $\Delta J = 1, 2, 3$ for Nd, Sm, Ho, Er and Tm complexes are magnetic and electric dipole forbidden in the zeroth order and are only allowed to first order in the interconfigurational operator (V_u) which mixes the *gerade* 5d states into the *ungerade* 4f electronic states as well as in the intraconfigurational V_g operator leading to the crystal field splitting. The $^4I_{9/2} \longrightarrow {}^2H_{9/2}$ transition with $\Delta S = 1$; $\Delta L = 1$; $\Delta J = 0$ for the Nd complex is both magnetic and electric dipole allowed to the first order in the spin–orbit coupling (H_{so}) and V_u. According to Richardson's classification,[14] the dissymmetry factors of the

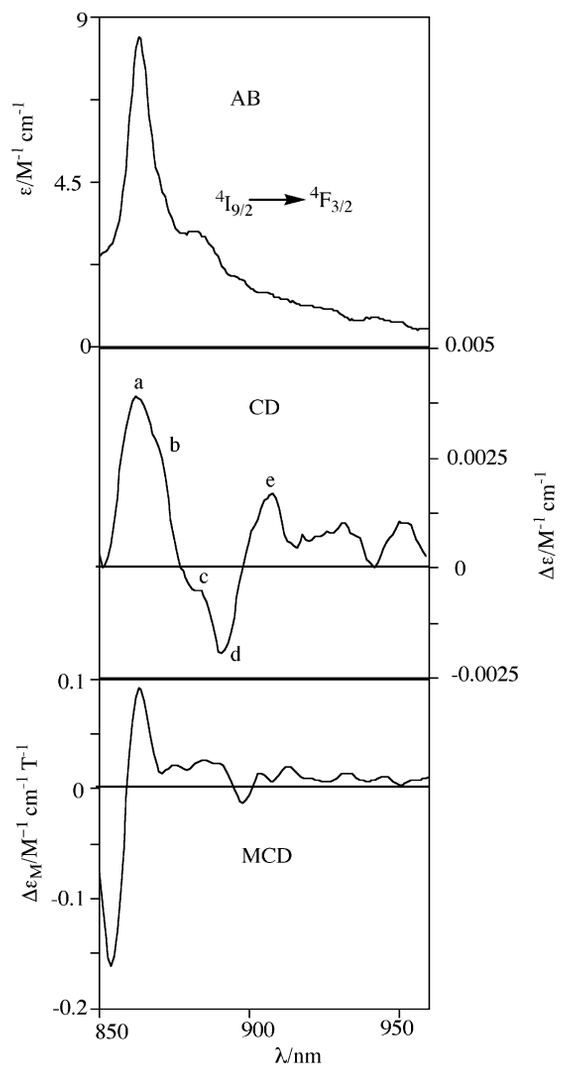

Fig. 2 NIR absorption (AB) (top) and NIR CD spectra (middle) of (Λ-Δ)-[$Cr(acac)_2$(ox)$Nd(HBpz_3)_2$] and NIR MCD of [$Cr(acac)_2$(ox)-$Nd(HBpz_3)_2$] (bottom) in CH_2Cl_2 (λ 850–960 nm).

former Nd, Sm, Ho, Er and Tm transitions are grouped as DIII class (types 3 and 5), while the latter Nd transition belongs to the DII class (type 9). Since the *g* values of the DIII and DII classes are qualitatively dependent on (V_g/V_u) and $(V_u)^{-1}$ where $1 > V_g > V_u$, respectively, the *g* values of the DIII class are smaller than those of the DII class.

Multiple CD components were observed for the 4f–4f transitions of Nd(III) in (Λ-Δ)-Cr(ox)Nd in the 700–960 nm region. These components are the first observation of NIR CD of the Nd(III) ion. The longest wavelength CD bands corresponding to the $^4I_{9/2} \longrightarrow {}^4F_{3/2}$ transition for the $4f^3$ electronic configuration of Nd(III) were observed at 850–960 nm with a major CD component with $g = +2.3 \times 10^{-4}$ as shown in Fig. 2. For the $^4I_{9/2} \longrightarrow$

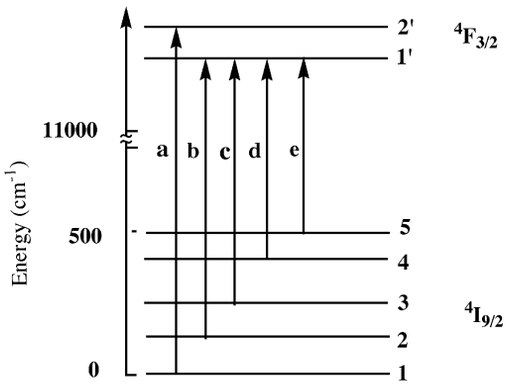

Fig. 3 Energy level diagram showing the transitions from the ground Kramers $^4I_{9/2}$ levels to the excited Kramers $^4F_{3/2}$ levels (a–e) corresponding to the tentatively assigned levels in Fig. 4.

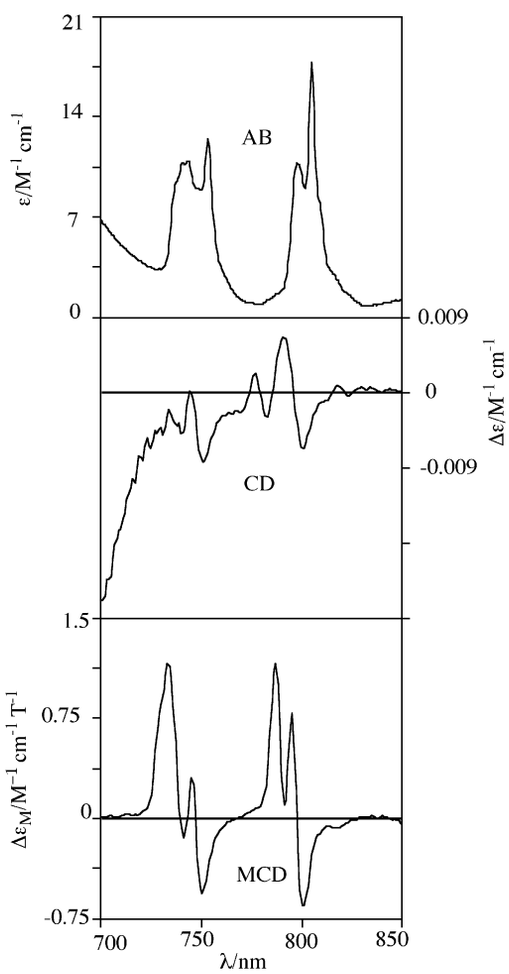

Fig. 4 NIR absorption (AB) (top) and NIR CD spectra (middle) of (Λ-Δ)-[Cr(acac)$_2$(ox)Nd(HBpz$_3$)$_2$] and NIR MCD of [Cr(acac)$_2$(ox)-Nd(HBpz$_3$)$_2$] (bottom) in CH_2Cl_2 (λ 700–850 nm).

$^4F_{3/2}$ transition the energy level diagram and tentative assignment of the sublevels (a–e) are depicted in Fig. 3. The $^4I_{9/2}$ ground state and the $^4F_{3/2}$ excited state are split into five and two Kramers levels, respectively, due to the crystal field. The CD components and the corresponding transitions are designated by (a–e) as in Figs. 2 and 3. The strongest CD band within the overlap region of the $^4I_{9/2} \longrightarrow {}^4F_{5/2}$ (DIII) and the $^4I_{9/2} \longrightarrow {}^2H_{9/2}$ (DII) transitions was observed at 770–820 nm as shown in Fig. 4. Unlike the Dy and Yb complexes of which the 4f–4f transitions belong to the DIII and DII classes, respectively, the $^4I_{9/2} \longrightarrow {}^4F_{5/2}$ and $^4I_{9/2} \longrightarrow {}^2H_{9/2}$ transitions of the Nd(III) complex

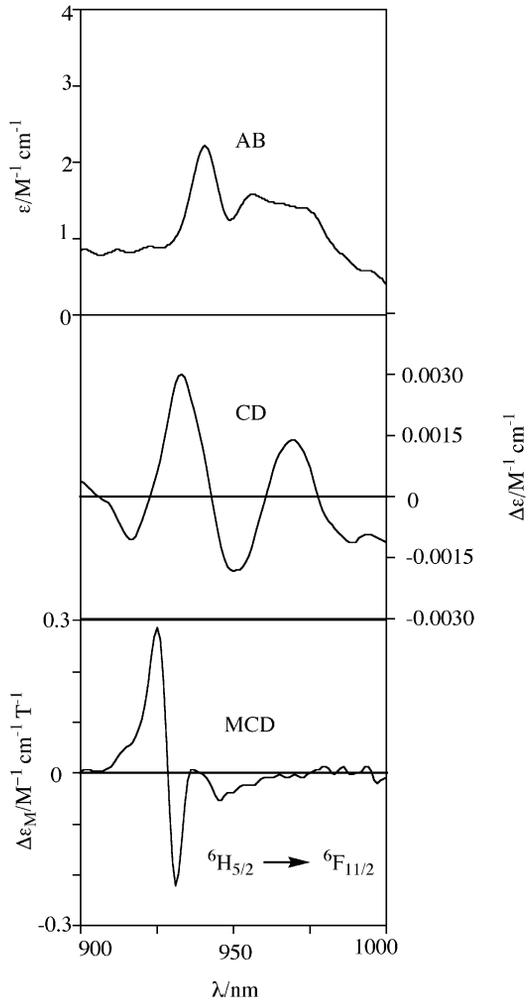

Fig. 5 NIR absorption (AB) (top) and NIR CD spectra (middle) of (Λ-Δ)-[Cr(acac)$_2$(ox)Sm(HBpz$_3$)$_2$] and NIR MCD of [Cr(acac)$_2$(ox)Sm(HBpz$_3$)$_2$] (bottom) in CH_2Cl_2.

are not distinguisable[12] by the CD intensity ($g = 6.6 \times 10^{-4}$) observed in this region. This may result from mutual cancellation due to the extensive overlap of the closely lying CD components, which thus leads to the apparent violation of the selection rule for the optical activity of the 4f–4f transitions. Shorter wavelength CD bands assignable[23] to the $^4I_{9/2} \longrightarrow {}^4F_{7/2}$ and $^4I_{9/2} \longrightarrow {}^4S_{3/2}$ transitions were clearly observed in the 740–744 nm and 739–740 nm regions, respectively, with the reduction of CD intensity due to the effect from the lower energy negative component of the d–d CD band[12] of the Cr(III) chromophore in the (Λ-Δ)-Cr(ox)Nd complex. For the $^6H_{5/2} \longrightarrow {}^6F_{11/2}$ (DIII) transition of Sm(III) in the (Λ-Δ)-Cr(ox)Sm complex, CD bands with a number of components were observed at 900–1000 nm with $g = ca.\ 1.5 \times 10^{-3}$ for the major CD component as shown in Fig. 5. In the $^5I_8 \longrightarrow {}^5I_5$ transition of Ho(III) in the (Λ-Δ)-Cr(ox)Ho complex, multiple CD components corresponding to the absorption bands were observed with a major CD component at 890 nm with $g = ca.\ 1.7 \times 10^{-4}$ as depicted in Fig. 6.

For the Er(III) ion in (Λ-Δ)-Cr(ox)Er, two CD bands corresponding to the $^4I_{15/2} \longrightarrow {}^4I_{11/2}$ transition at 975 nm and the $^4I_{15/2} \longrightarrow {}^4I_{9/2}$ transition at *ca.* 750–900 nm with the major CD component at *ca.* 802 nm were observed as shown in Figs. 7 and S3, † respectively. The *g* values for the major CD components are found to be 2.3×10^{-3} and 1.1×10^{-4} respectively, both corresponding to the DIII transitions. For (Λ-Δ)-Cr(ox)Tm, multiple CD components were clearly observed in the *ca.* 750–800 nm region with $g = 2 \times 10^{-4}$ for the $^3H_6 \longrightarrow {}^3H_4$ (DIII) transition as shown in Fig. 8, even though the CD band is also affected by

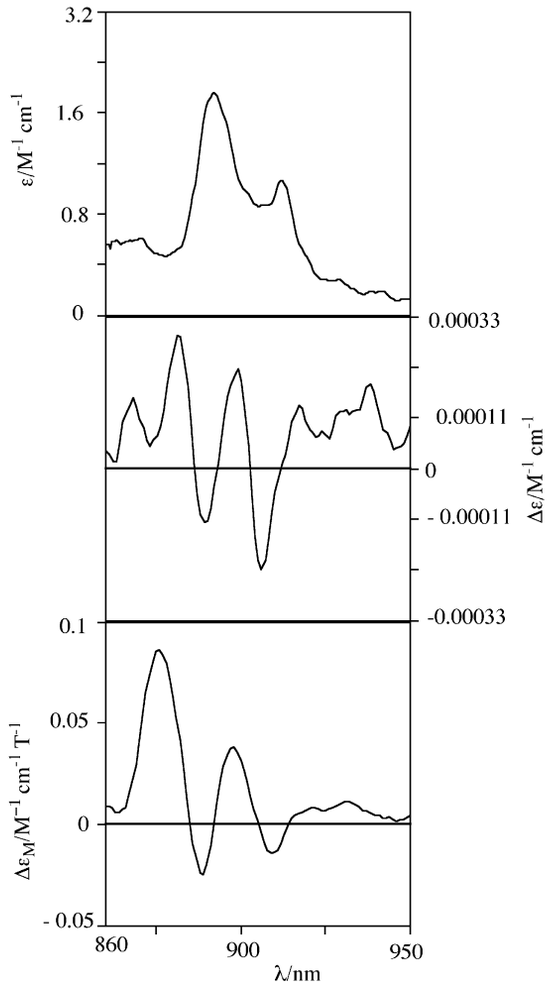

Fig. 6 NIR absorption (AB) (top) and NIR CD spectra (middle) of (Λ-Δ)-[Cr(acac)$_2$(ox)Ho(HBpz$_3$)$_2$] and NIR MCD of [Cr(acac)$_2$(ox)-Ho(HBpz$_3$)$_2$] (bottom) in CH_2Cl_2.

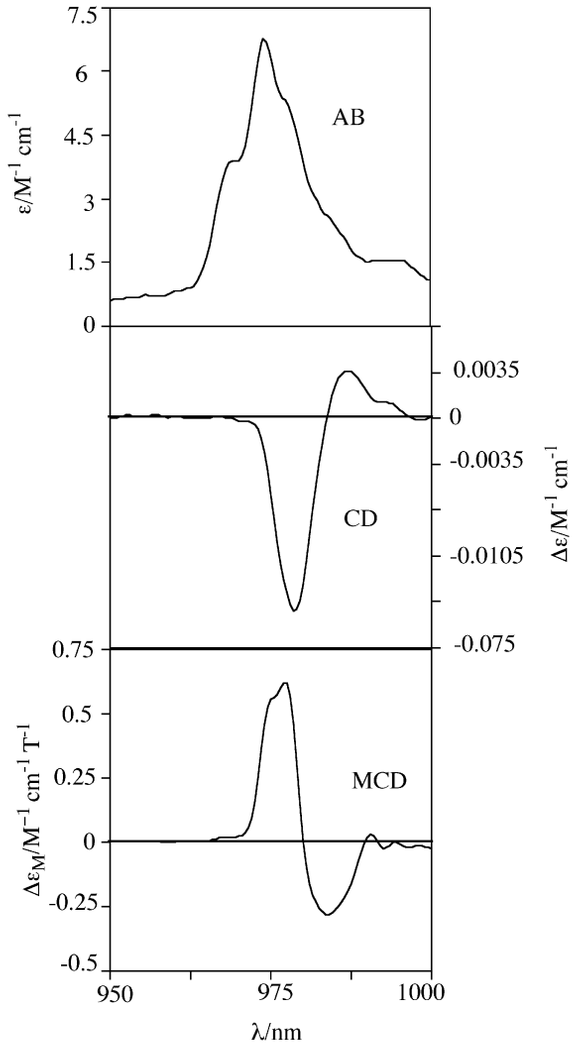

Fig. 7 NIR absorption (AB) (top) and NIR CD spectra (middle) of (Λ-Δ)-[Cr(acac)$_2$(ox)Er(HBpz$_3$)$_2$] and NIR MCD of [Cr(acac)$_2$(ox)-Er(HBpz$_3$)$_2$] (bottom) in CH_2Cl_2 (λ 950–1000 nm).

the negative minor component of the d–d CD band of the Cr(III) chromophore in Cr(ox)Tm. This diversity in components may be due to Tm having the largest crystal field splitting[24] among the lanthanide(III) ions under study. The dissymmetry factors were found to be of an order of 10^{-3} to 10^{-4} for all the Cr(ox)Ln complexes signifying the configurational chirality around lanthanide ions[12] in solution.

Inspection of the CD patterns of the (Λ-Δ)-Cr(ox)Ln (Ln = Nd, Sm, Ho, Er and Tm) complexes indicates some similarities in sign of the 4f–4f transitions which belong to the DIII class. It follows that the major CD band in the highest energy region for all the 4f–4f transitions with DIII class of the (Λ-Δ)-Cr(ox)Ln assemblies shows a positive CD sign including the Dy(III)[12] complex, except for the $^4I_{15/2} \longrightarrow {}^4I_{11/2}$ transition at 975 nm in the (Λ-Δ)-Cr(ox)Er complex as shown in Fig. 7. This may be a common criterion for the relationship between the CD signs in the 4f–4f transitions and the absolute configuration around the Ln(HBpz$_3$)$_2$(ox) moiety; a positive sign to indicate the Δ absolute configuration as has been observed for the Yb(III) complexes with chiral DOTMA ligands.[11]

NIR MCD

The present NIR MCD spectra in the 800–1000 nm region of the racemic Cr–Ln complexes are the first observed to date, though there have been a few NIR MCD data in the region up to 800 nm reported.[3–5] A group of MCD components of a few Nd(III) complexes in the 740 nm region in solution were reported,[5] which are assigned to the $^4I_{9/2} \longrightarrow {}^4S_{3/2}$ transition. The shortest wavelength MCD component in this region near 735 nm has a positive sign for all the complexes.[5] This is in accordance with the present solution MCD spectra of the Cr–Nd complex as in Fig. 2. The first solution MCD spectrum in the longer wavelength region (>800 nm) corresponding to the $^4I_{9/2} \longrightarrow ({}^2H_{9/2}, {}^4F_{5/2}$ and $^4F_{3/2})$ transitions of the Cr(ox)Nd complex was observed in CH_2Cl_2, though the solid state MCD spectra of Nd ions in doped $LiNbO_3$ crystal systems have already been reported.[3] Apart from the Nd complex, the racemic Cr(ox)Ln complexes show prominent MCD multiple components in positions similar to the highest peaks of the absorption and CD spectra (Figs. 5–8). It is noted that the shortest wavelength MCD components are most manifest in the spin-allowed transitions with $\Delta J = 3$; the $^4I_{9/2} \longrightarrow {}^4F_{3/2}$ for the Nd, the $^6H_{5/2} \longrightarrow {}^6F_{11/2}$ for the Sm and the $^4I_{15/2} \longrightarrow {}^4I_{9/2}$ for the Er complex. As for the key CD component related to the absolute configuration, most of the corresponding MCD components give positive A terms except for the Nd and Er complexes as shown in Figs. 2 and 4–8.

Conclusions

The X-ray structural analysis and NIR CD studies show that the stereospecific formation and configurational chirality is retained around the light Ln(III) ions as well as around the

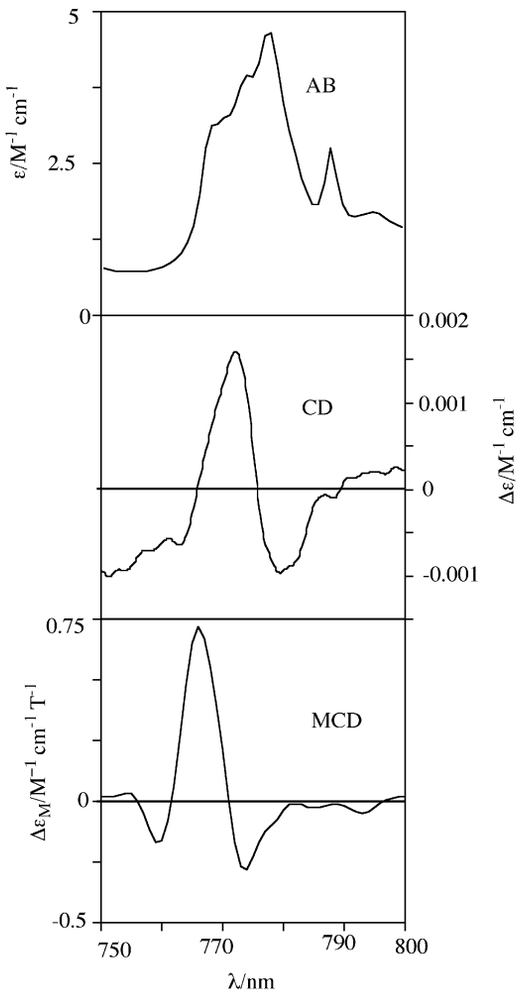

Fig. 8 NIR absorption (AB) (top) and NIR CD spectra (middle) of (Λ-Δ)-[$Cr(acac)_2(ox)Tm(HBpz_3)_2$] and NIR MCD of [$Cr(acac)_2(ox)$-$Tm(HBpz_3)_2$] (bottom) in CH_2Cl_2.

heavy Ln(III) ions in the Cr(ox)Ln assemblies. The CD in the 4f–4f transitions of these structurally well characterized complexes enables us to propose a criterion to determine the absolute configuration; a positive sign for the Δ absolute configuration in support of the NIR absorption and MCD spectra which confirm the positions and the relative intensities of the 4f–4f transitions. In almost all cases, the better resolved CD spectra in the electronic transitions were observed than either the NIR absorption or MCD bands.

Acknowledgements

We gratefully acknowledge support of this research by a Grant-in-Aid for Scientific Research (No. 10304056) from the Ministry of Education, Science and Culture.

References

1 (*a*) B. Norden and I. Grenthe, *Acta Chem. Scand.*, 1972, **26**, 407; (*b*) R. W. Schwartz, A. Banerjee, A. C. Sen and M. Chowdhury, *J. Chem. Soc., Faraday Trans. 2*, 1980, **76**, 620; (*c*) H. G. Brittain, *Coord. Chem. Rev.*, 1983, **48**, 243; (*d*) P. K. Chatterjee and M. Chowdhury, *Inorg. Chem.*, 1982, **21**, 2499.
2 P. Biscarini, *Inorg. Chim. Acta*, 1983, **74**, 65.
3 (*a*) B. Briat, *C. R. Hebd. Seances Acad. Sci.*, 1965, **260**, 853; (*b*) B. Briat, *C. R. Hebd. Seances Acad. Sci.*, 1965, **260**, 3335; (*c*) B. Briat, M. Billardon and J. Badox, *Anal. Chim. Acta*, 1966, **34**, 465.
4 (*a*) C. Görller-Walrand and J. Godedmont, *J. Chem. Phys.*, 1977, **67**, 48; (*b*) C. Görller-Walrand and J. Godedmont, *J. Chem. Phys.*, 1977, **67**, 3655; (*c*) C. Görller-Walrand, Y. Beyens and J. Godedmont, *J. Chim. Phys.*, 1979, **76**, 192; (*d*) C. Görller-Walrand, H. Peeters, Y. Beyens, N. D. Moitie-Neyt and M. Behets, *Nouv. J. Chim*, 1980, **4**, 715; (*e*) C. Görller-Walrand, P. Verhoeven, J. D. Olieslager, L. Fluyt and K. Binnemans, *J. Chem. Phys.*, 1994, **100**, 815.
5 J. P. Sipe III and R. B. Martin, *J. Inorg. Nucl. Chem.*, 1974, **36**, 2122.
6 (*a*) Y. Kato and M. Asano, *Bull. Chem. Soc. Jpn.*, 1979, **52**, 999; (*b*) C. Bonardi, R. A. Carvalho, H. C. Basso, M. C. Terrile, G. K. Cruz, L. E. Bausa and J. Garcia Sole, *J. Chem. Phys.*, 1999, **111**, 6042.
7 E. Huskowska and J. P. Riehl, *Inorg. Chem.*, 1995, **34**, 5615.
8 C. L. Maupin, R. S. Dickens, L. G. Govenlock, C. E. Mathieu, D. Parker, J. A. G. Williams and J. P. Riehl, *J. Phys. Chem. A*, 2000, **104**, 6709.
9 S. C. J. Meskers and H. P. J. M. Dekkers, *J. Phys. Chem. A*, 2001, **105**, 4589.
10 L. D. Bari, G. Pintacuda and P. Salvadori, *J. Am. Chem. Soc.*, 2000, **122**, 5557.
11 L. D. Bari, G. Pintacuda, P. Salvadori, R. S. Dickens and D. Parker, *J. Am. Chem. Soc.*, 2000, **122**, 9257.
12 M. A. Subhan, T. Suzuki and S. Kaizaki, *J. Chem. Soc., Dalton Trans.*, 2001, **4**, 492.
13 (*a*) J. Costes, F. Dahan and A. Dupuis, *Inorg. Chem.*, 2000, **39**, 165; J. Costes, F. Dahan, A. Dupuis and J. Laurent, *Inorg. Chem.*, 2000, **39**, 169; (*b*) M. Sasaki, K. Manseki, H. Horiuchi, M. Kumagai, M. Sakamoto, H. Sakiyama, Y. Nishida, M. Sakai, Y. Sadaoka, M. Ohba and H. Okawa, *J. Chem. Soc., Dalton Trans.*, 2000, 259; (*c*) S. Rigault, C. Piguet and J. G. Bunzli, *J. Chem. Soc., Dalton Trans.*, 2000, 2045; (*d*) Y. Cui, Y. Qian and J. Huang, *Polyhedron*, 2001, **20**, 1795.
14 F. S. Richardson, *Inorg. Chem.*, 1980, **19**, 2806.
15 S. Trofimenko, *J. Chem. Soc.*, 1967, **89**, 3170.
16 T. Sanada, T. Suzuki, T. Yoshida and S. Kaizaki, *Inorg. Chem.*, 1998, **37**, 4712.
17 P. Choppens, L. Leiserowitz and D. Rabinovich, *Acta Crystallogr.*, 1965, **18**, 1035.
18 G. M. Sheldrich, *Acta Crystallogr., Sect. A*, 1990, **46**, 467.
19 G. M. Sheldrich, SHELXL97, University of Göttingen, Germany, 1997.
20 TeXsan, Single Crystal Structure Analysis Software, ver. 1.9, 1998, Molecular Structure Corporation and Rigaku Co. Ltd., MSC, The Woodlands, TX 77381-5209, USA and Rigaku Co. Ltd., Akishima, Tokyo 196-8666, Japan.
21 H. D. Flack, *Acta Crystallogr., Sect. A*, 1983, **39**, 876.
22 C. K. Johnson, ORTEP II, Report ORNL-5138, Oak Ridge National Laboratory, Oak Ridge, TN, 1976.
23 W. T. Carnall, P. R. Fields and K. Rajnak, *J. Chem. Phys.*, 1968, **49**, 4424.
24 B. M. Alsaadi, R. J. C. Rossotti and R. J. P. Williams, *J. Chem. Soc., Dalton Trans.*, 1980, 2151.
25 M. G. B. Drew, *Coord. Chem. Rev.*, 1977, **24**, 2151.